Sustainable Environment Research

RESEARCH Open Access

Enhanced photocatalytic performance of Nb doped TiO_2/reduced graphene oxide nanocomposites over rhodamine B dye under visible light illumination

Neradabilli Prabhakarrao, Tirukkovalluri Siva Rao*, Kapuganti Venkata Divya Lakshmi, Gorli Divya, Genji Jaishree, Imandi Manga Raju and Shaik Abdul Alim

Abstract

The present study discusses the synthesis of Nb doped TiO_2/reduced graphene oxide (rGO) intercalated nanocomposites via sol-gel route at a lower temperature by using different loading amounts of graphene oxide (GO) (1 to 10 wt%). The synthesized composite materials were further characterized by copious instruments such as X-ray Diffractometer, UV-Vis Diffuse Reflectance Spectroscopy, Scanning Electron Microscopy, Transmission Electron Microscopy, Brunauer-Emmett-Teller surface area analysis, Raman and Fourier Transform-Infrared Spectroscopy. The experimental results stated that the Nb doped TiO_2 nanoparticles uniformly distributed on the surface of rGO with an interfacial linking bond between TiO_2 and rGO. Later, the photocatalytic degradation of Rhodamine B (RhB) dye using produced materials under visible light irradiation was examined. These results revealed that Nb doped TiO_2/rGO nanocomposites exhibited better photocatalytic performance than Nb doped TiO_2 for the removal of RhB dye. However, among all, the nanocomposite having 5 wt% of GO content achieves the highest degradation efficiency for RhB dye approximately 98% under visible light exposure. Altogether, the unique properties such as electron accepting and transporting properties of GO in the nanocomposite is caused to enhance photocatalytic activity by minimizing the charge carrier's recombination rate.

Keywords: Graphene oxide, Niobium, Photocatalysis, Rhodamine B dye, Titanium oxide

Introduction

From the past few decades, textile wet processing and finishing industries are strongly dependent on synthetic dyes that severely contaminating water as they produce organic pollutants. Cleansing of wastewater produced from these industries is attracting more importance in modern days due to toxic, low biodegradable, high persistence and carcinogenic nature of the dye pollutants [1, 2]. Thus, an effective and economically feasible treatment technique is necessary for removing dyes from the textile wastewater. Apart from the various conventional methods developed, advanced oxidation process is largely adopted method for remediation of dye contaminated effluents because of its flexibility, efficacy and relatively low expensive. Semiconductor-mediated photocatalytic oxidation has been used extensively to abolish the organic pollutants from its contaminated wastewater into H_2O and CO_2, etc. through oxidation-reduction interactions between organic pollutants and photogenerated reactive oxygen species [3].

Titania (TiO_2) has been generally admitted as a promising photocatalyst for the decomposition of hazardous environmental impurities owing to its unique physical and chemical properties [4]. However, due to large band-gap 3.2 eV (anatase TiO_2) and poor electron mobility, it

* Correspondence: sivaraoau@gmail.com
Department of Inorganic and Analytical Chemistry, Andhra University, Visakhapatnam 530003, India

shows very limited photosensitization in the visible range of solar spectrum. To overcome these challenges, several efforts have been made by researchers such as transition metal doping [5, 6], semiconductor coupling [7], surface polymer sensitization [8, 9] and combination with supporting materials such as carbonaceous materials [10]. In particular, metal ion doping of TiO_2 along with carbonaceous material combination is the emerging area in present era. Doping can narrow the bandgap and carbonaceous material can limit the charge carriers (e^--h^+ pair) recombination [11]. Several investigators reported doping of TiO_2 lattice with transition metal ions, i.e., Cr, Cu, Zr, Ce, Sn, Fe, and Ni etc. [12]. Presently, as compare with many dopants, Nb doped TiO_2 (NT) has attracted greater attention because of its utilization in various applications like photocatalysis, dye sensitized solar cells, sensors, fuel cell catalysis, and transparent conductive films [12]. It is mainly due to the ionic radius of Nb^{5+} (0.064 nm) is significantly larger than Ti^{4+} (0.0605 nm) which effectively constricts the band gap of TiO_2 to enlarge its adsorption in visible region and on the other side metals are thermally unstable as well as effortless to cause the charge carriers recombination [13].

Given on this obstacle, numerous experiments have been conducted by researchers and achieved efficient photocatalyst by providing support to TiO_2 nanoparticles such as multiwall carbon nanotubes because its multiple graphene layers contact with TiO_2 allow electrons can flow through, which accelerate the photogenerated charge carriers separation more favourably [14]. Significant results have been obtained using graphene as 2-D supporting material to catalyst due to its single atomic thick 2-D hexagonal lattice sheet structure aligned by a sp^2-hybridized carbon network and its wide variety of features such as electrical, thermal, and mechanical [15]. Because of the hydrophobic nature of graphene, strong intercalation of metal oxide on graphene surface is difficult. In spite of this, chemically modified graphene-based materials like graphene oxide (GO) and reduced graphene oxide (rGO) drawing more attention in semiconductor photocatalysis as supporting material. The existing oxygen functionalities in GO and rGO, like carbonyl (C=O), hydroxyl (O-H), epoxide (C-O-C) groups making graphene to display wonderful hydrophilic character and good intercalation chemistry [16]. It appears reasonable that greater advancement in photocatalytic performance can be achieved by the novel Nb doped TiO_2/rGO composite (NTG) material with high interfacial contact and potential.

Herein, this paper demonstrated the synthesis of NTG nanocomposite by altering the GO loads using modified sol-gel method via in-situ process at low temperature. Improvement in the photocatalytic efficiency of NTG catalysts caused by GO insertion was orderly investigated depending upon the electronic structure, optical absorption, microstructure, and electrochemical behaviours. The photocatalytic activity of the NTG nanocomposites has been assessed by degrading the Rhodamine B (RhB) under visible light exposure.

Materials and methods

Chemical reagents

Reagents included Titanium tetra n-butoxide (TTBO) (E-Merck, Germany) and Niobium Chloride ($NbCl_5$) (Koch-light Laboratories), sodium nitrate ($NaNO_3$), potassium permanganate ($KMnO_4$), 36.0–38.0% of hydrochloric acid (HCl) and 95.0–98.0% of sulphuric acid (H_2SO_4), ethanol and hydrogen peroxide (H_2O_2) were obtained from E-Merck (India). Graphite (99%) flakes purchased from Sigma Aldrich, USA, RhB dye from HI-Media, India. For solutions preparation, doubly distilled water was used. All these specified chemicals were analytical grade reagents used without further purification.

Nb doped TiO_2/rGO nanocomposite synthesis

The modified hummer's method was adopted to synthesize GO [17] and explained in Supplementary information (SI) in detail. As per the earlier reported method by the author [18], NTG composites were synthesized via sol-gel approach by dispersing different GO concentrations from 1 to 10 wt% weight ratios and fixed Nb loading as 5 wt% corresponding to Ti at low temperatures (Fig. 1). In a typical synthesis route, $NbCl_5$ and TTBO were chosen as source materials for Nb and Ti respectively. At first, required amount of Nb (5 wt%) was added into 50 mL of ethanol solution stirred for 30 min and then 15 mL TTBO was mixed simultaneously and resultant noted as solution I. Next, GO taken into 50 mL of ethanol (containing 1 wt% of GO relevant to Ti) underwent ultrasonication for 1 h to obtain homogeneous GO suspension named as solution II. These two solutions were mixed vigorously by the slow addition of solution I into solution II, followed by the addition of a mixture of 2 mL water and 1 mL nitric acid dropwise through the burette and continuous stirring for more than 1 h and was aged at 25 °C until gel formation has occurred. The resulting wet gel was dried at 70 °C in a hot air oven for 24 h and labelled as NTG1. The same procedure was adopted for synthesis of NTG5, NTG10 and NT by varying the GO concentrations in colloidal suspension from 5 wt% GO, 10 wt% GO and without GO respectively.

Characterization techniques

The instruments used to characterise the synthesized materials are X-ray diffractometer (XRD, Bruker) using

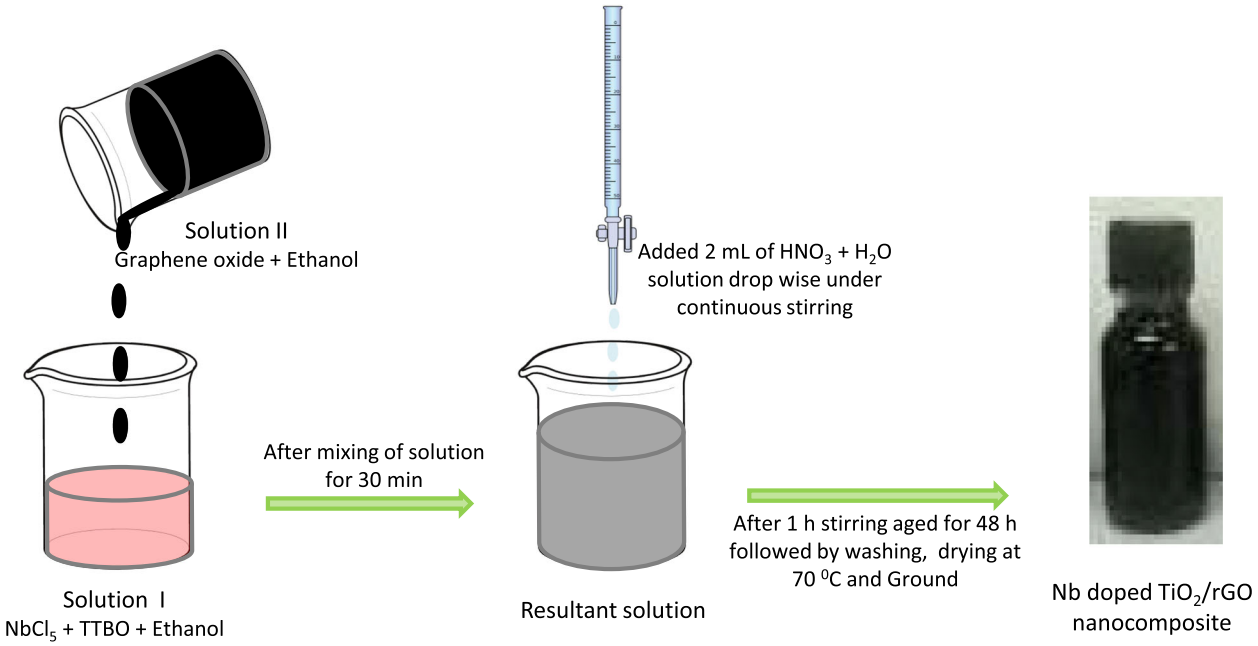

Fig. 1 Schematic representation of synthesis of Nb doped TiO_2/rGO nanocomposite

Cu-Kα radiation operated at 30 kV and 30 mA over at 2 ° min^{-1}, UV-Visible diffuse reflectance spectrophotometer (DRS) (Scinco Co., S-3100) using $BaSO_4$ as reference material over the spectral range of 200–800 nm, scanning electron microscopy (SEM, JSM-6610 LV), transmission electron microscopy (TEM, JEOL 120 KV), Brunauer-Emmett-Teller (BET) (Quantachrome Nova version 10.0), and X-ray photoelectron spectroscopy (XPS, PHI quantumESCA microprobe system) using the Al-Kα line of a 250-W X-ray tube as a radiation source with an energy of 12,536 eV, current of 16 mA and voltage of 12.5 kV. Raman measurements are noted using RM2000 Raman spectrometer. Fourier Transform Infra-Red (FT-IR, Shimadzu IR prestige 21) spectrophotometer over the frequency range of 400–4000 cm^{-1} with KBr pellets as a reference and photoluminescence (PL) spectra were obtained using fluorescence spectrophotometer (Hitachi, F-7000, Japan). The decomposition kinetics for the photocatalytic activity of nanocomposites was studied by UV-Visible spectrophotometer (UV-2200, Shimadzu, Japan).

Photocatalytic activity of nanocomposites

Photocatalytic decomposition capabilities of NTG catalysts were evaluated under visible light illumination by taking RhB as model dye pollutant and experiments were performed in a photoreactor which consists of 400 W mercury high-pressure vapor lamp used as visible light source. In brief, initially 50 mg of catalyst was dispersed in 100 mL (2 mg L^{-1}) of RhB aqueous solution. After stirring under dark conditions for 30 min to attain adsorption-desorption equilibrium, the light was switched on. A sample of 5.0 mL was collected at regular time intervals and the photocatalyst particles were separated by centrifugation from collected suspension prior to analysis. The change in RhB dye concentration was measured by absorbance at 543 nm using a UV-Visible spectrophotometer. The extent of photodegradation efficiency of catalysts was calculated by obtaining the relationship between C/C_0 and illumination time (min), here C and C_0 are the concentrations of RhB dye at time t and time zero respectively. The RhB concentration changes (C/C_0) were directly proportional to absorbance changes (A/A_0) during photodecomposition; the % of RhB degradation was calculated using Eq. (1).

$$\%\text{of Photo degradation} = \left(1 - \frac{\text{At}}{\text{A0}}\right) * 100 \quad (1)$$

where A_0 is the absorbance of RhB at an initial time and A_t is the absorbance of RhB at a time 't' during the degradation process.

Results and discussion

XRD analysis

As shown in Fig. 2, XRD analyses of various samples such as graphite, GO, and NTG composites were carried out. The diffraction peak centred at $2\theta = 26.19°$ was found a clear (002) orientation of pure graphite with an interlayer spacing of 0.34 nm as depicted in

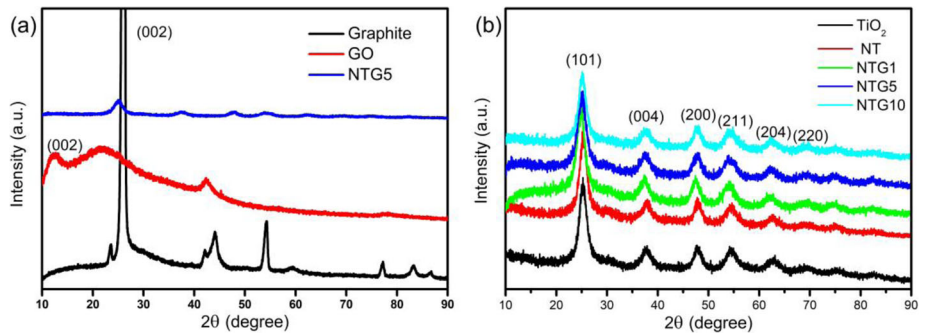

Fig. 2 XRD patterns of Graphite, GO and NTG nanocomposites

Fig. 2a. The formation of GO was confirmed by the appearance of the new peak at $2\theta = 12.68°$ with an interlayer distance of 0.699 nm corresponding to the (002) lattice plane [15].

Comparison of XRD results of pristine TiO_2 with that of the NT and NTG composites reveals that all diffraction patterns essentially identical as evident from Fig. 2b. All the discerned peaks for NTG nanocomposites at $2\theta = 25.06$, 37.27, 47.99, 54.8, 62.32 and 68.8° can be signed to the respective anatase crystal faces of (101), (004), (200), (211), (204) and (220) which is in well concord with the JCPDS No. 21–1272. The relevant peaks for rutile and brookite phases are absent which are usually appeared at $2\theta = 27.3°$ and $2\theta = 30.8°$ in all XRD patterns of NTG composites implying that formation of pure anatase TiO_2 at low temperatures. Also, the absence of reflections from impurity phases, i.e., from Nb_2O_5 or NbO_2 suggested that proper doping of Nb into TiO_2 lattice occurred. There is no significant peak relevant to rGO observed in composites which might be due to the relatively low concentration of GO in the composites capped by the strong (101) diffraction signal from crystalline TiO_2. Furthermore, the existence of rGO in NTG5 nanocomposites can be explained clearly in the Raman analysis. It can be noticed from the Fig. 2b that the slight broadening in peak width with the introduction of GO (Fig. 2b) occurred. The average crystalline size of NTG composites is smaller than that of pristine TiO_2 and NT which are estimated by using Debye-Scherrer's formula with respect to anatase peak as given in Table 1. It is inferred that, because of the attained strong interactions between TiO_2 and graphene during the hydrolysis of sol samples, the agglomeration of the TiO_2 crystalline particles can be reduced [19].

UV-vis/DRS analysis

From Fig. 3a, a significant influence on optical absorption of NTG nanocomposites has been observed by varying GO loads. Meanwhile, for NTG nanocomposites a red shift towards higher wavelength with strong and broad absorptions in the visible region can be distinctly detected which indicates band gap narrowing of TiO_2 [20]. Besides, TiO_2 and NT spectra are showing relatively lower absorption intensity compared with NTG nanocomposites in the visible region. The optical bandgap of photocatalyst is calculated using the Tauc's relationship. The Eq. (2) for bandgap energy is described as below,

$$\sqrt{\alpha h\upsilon} = C(h\upsilon - Eg) \tag{2}$$

where, h is Planck's constant, υ is the frequency of light, C is the proportionality constant, α is the absorption coefficient at a certain wavelength λ of the solid, and E_g is the bandgap energy.

Fig. 3b displays the relationship between $(\alpha h\upsilon)^{1/2}$ and photon energy ($h\upsilon = 1239/\lambda$) for TiO_2, NT and NTG nanocomposites. 2.98 eV is the band gap observed for NT, whereas the bandgap of 2.68, 2.62 and 2.52 eV

Table 1 Average crystallite size (nm), band gap energy (eV), BET surface area ($m^2\,g^{-1}$) and mean pore diameter (nm) of each catalyst

Photocatalyst	Crystallite size (nm)	Band gap energy (eV)	BET surface area ($m^2\,g^{-1}$)	Mean pore diameter (nm)	Pore volume ($cm^3\,g^{-1}$)
NT	58.2	2.98	209	5.62	0.29
NTG1	30.7	2.68	250	4.03	0.25
NTG5	29.6	2.62	257	4.24	0.28
NTG10	31.7	2.52	238	3.79	0.23

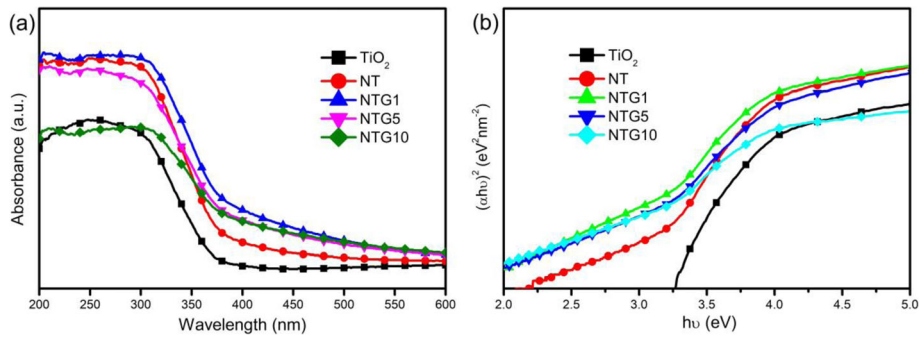

Fig. 3 **(a)** The UV-Vis diffuse reflectance absorption spectra and **(b)** corresponding Tauc's plot of NTG nanocomposites compared with NT

correspond to NTG1, NTG5 and NTG10 respectively, i.e., bandgap energy decreases with increase in GO content. These results evident (Table 1) that compared to the bare TiO_2 and NT, red shift was quantitatively observed in NTG nanocomposites. The interactions between π electrons of GO and the existed surface free electrons of NT are accountable for the formation of the Ti-O-C bond structure, which subsequently caused in the band gap energy reduction of nanocomposites [20].

SEM-EDX and TEM analyses

The resultant SEM, TEM and HR-TEM images for GO and NTG5 nanocomposite are depicted in Fig. 4. From SEM image of typical GO displayed in Fig. 4a, graphene sheets were observed which implied the presence of kinked and wrinkled shaped structures that were corrugated and scrolled intrinsic to graphene sheets [21]. Figure 4b presents the representative view of exfoliated GO, the observed crumples and folds in image suggesting the presence of typical single layered or multilayered GO. The existing functional groups on GO sheets could support for nucleation and uniform growth of nanoparticles by providing reactive and anchoring sites [22]. It can be clearly identified from the TEM image (Fig. 4c) of NTG5 nanocomposite that, it consists of a large amount of the spherically shaped NT nano particles (np's) which are uniformly anchored onto rGO sheet surface without obvious agglomeration. It can also see that, NTG5 had the

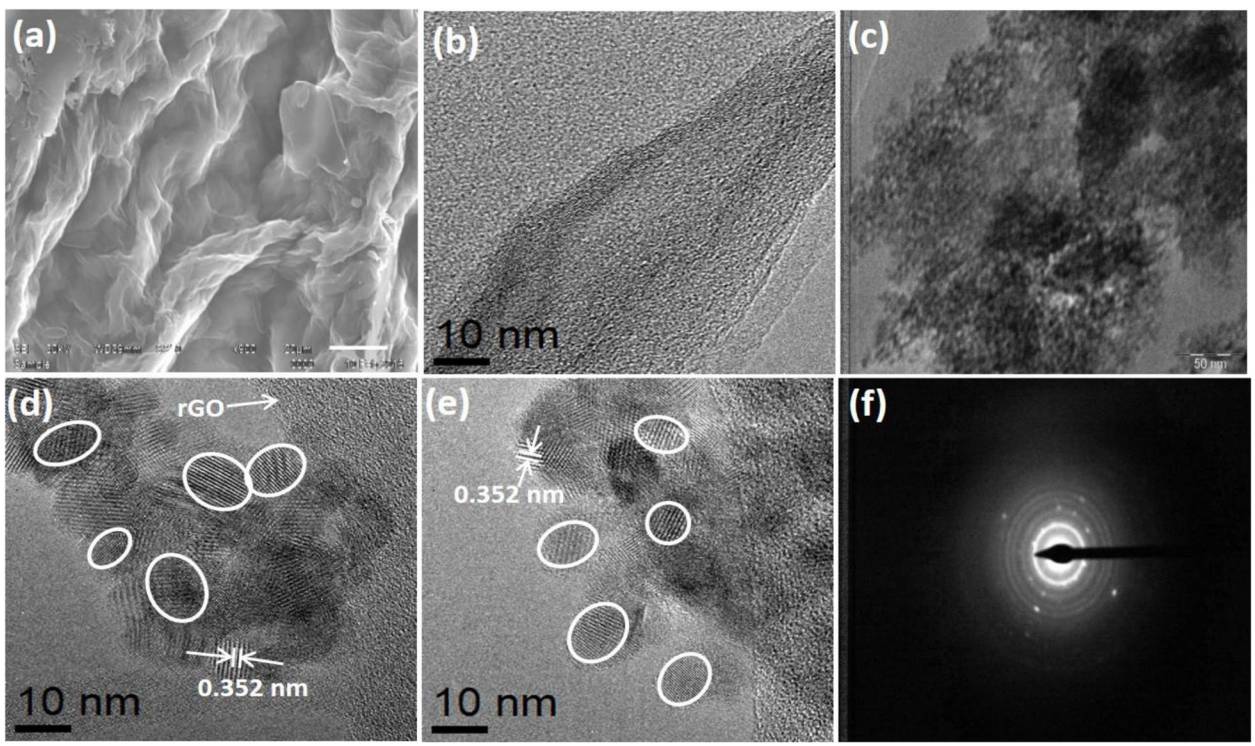

Fig. 4 **(a)** SEM image of GO, **(b)** HRTEM images of GO, **(c)** TEM image of NTG5, **(d)** and **(e)** are HR-TEM images of NTG5, **(f)** SAED patterns of NTG5

smallest particle size (approximately 5–10 nm) due to the hindering effects of rGO on the growth of NT np's. Altogether, the interaction between NT np's and rGO suggests that a complete conduction network could attain throughout the NTG5. This would allow injecting photogenerated electrons from NT np's into the rGO sheets upon which they are anchored and the electrons to flow through the graphene network within the composite rather than passing through the NT np's themselves. This could significantly cause enhancement in the photocatalytic efficiency of the photocatalyst. Figure 4d and e depict the HR-TEM images of NTG5 nanocomposite and unequivocal reveals that the specific interplanar spacing is 0.35 nm belonging to the (101) plane of anatase TiO_2, which is coincident with the results of XRD. The identification of crystalline fringes in rGO sheets is impossible due to the ultrathin structural network of rGO. From the SAED patterns of NTG5 (Fig. 4f), it was found that a typical 6-fold symmetric diffraction pattern observed in the NTG5 catalyst. Furthermore, the existence of the polycrystalline structure of TiO_2 in composites is matched with the XRD analysis results. Notably, any additional pattern in SAED corresponding to the crystalline impurities was not observed.

EDX spectra of NT and NTG5 are given in Fig. S1. EDX spectrum of NTG5 (Fig. S1a) demonstrates the presence of Ti, O, and C mainly along with small quantities of dopant Nb which is significant to the successful generation of highly pure nanocomposite. Mainly, the signals for C and Ti could have emerged from the rGO sheets and the TiO_2 nanoparticles, respectively. Following, the signal for O could be arisen from both TiO_2 and rGO because of its oxygen-containing functional groups. The elemental microanalysis of NT and NTG5 are summarized in Table S1.

BET analysis

Porosity and surface area of photocatalyst were described by nitrogen adsorption-desorption measurement. The nitrogen adsorption isotherms and distribution of pore sizes of NTG5 and NT np's can be found in Fig. 5. In accordance with the IUPAC representations, the microporous materials are having pore diameter smaller than 2 nm, substances having greater than 50 nm termed as macroporous materials; at last, substances lie in the middle fall under the mesoporous category and the isotherm of NTG5 nanocomposite shown in Fig. 5a corresponds to type IV classification and the type E hysteresis loop is an exceptionally matched with the De Boer classification ascribed to the mesoporous solid substances [23]. The obtained BET surface area (S_{BET}) and pore volume (Vp) of NT and NTG nanocomposites are tabulated in Table 1. Significantly, the surface area of NTG nanocomposites (238 to 257 $m^2\ g^{-1}$) is slightly greater than that of NT (209 $m^2\ g^{-1}$), it might be attributed to the deposition of NT np's on the surface of rGO in NTG5 nanocomposite. This may be attained either because of the rGO sheets stacking structure or by the insertion of rGO layers that minimizes the NT np's agglomeration. It can be seen that, there is no obvious difference in the BET surface area of the NTG nanocomposites by increasing GO loading has been found.

In addition, pore size distribution curves were plotted (Fig. 5b) which are calculated by the BJH (Barrett-Joyner-Halenda) method from the desorption isotherm. From the BJH plot of NTG5 nanocomposite, it can be understood that the majority of the pores lie below 10 nm and exhibits a peak at 3.32 nm denotes its mesoporous nature. Further, it is observed that the obtained average mean pore diameter of NTG5 and NT np's are 4.24 and 5.62 nm, respectively, lies under mesoporous which are distributed uniformly. Thus, the smaller pore diameter in NTG5 reflects its smaller particle sizes, coincides with the SEM and TEM characterization results. Therefore, greater S_{BET} and pore volume of NTG5 nanocomposite can efficiently provide the enhanced absorption of dye molecules on its surface in aqueous solution which results in an enhancement in photocatalytic degradation of dye.

XPS analysis

The signals correspond to the Ti, O, Nb and C species could be clearly identified from the full range spectrum

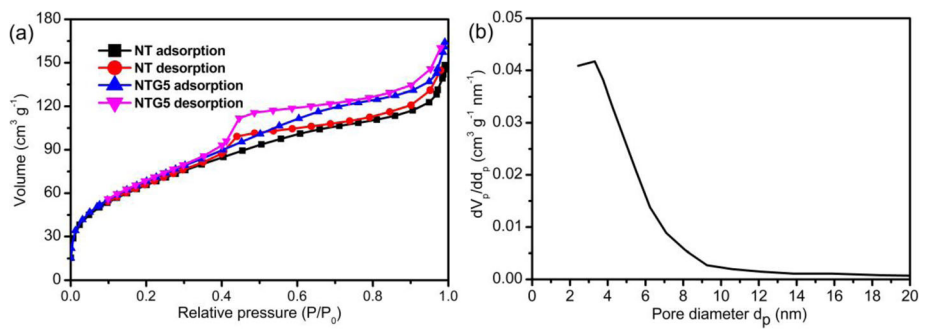

Fig. 5 **(a)** Nitrogen adsorption-desorption isotherms of NT and NTG5 photocatalysts and **(b)** The corresponding BJH pore size distribution plot of NTG5

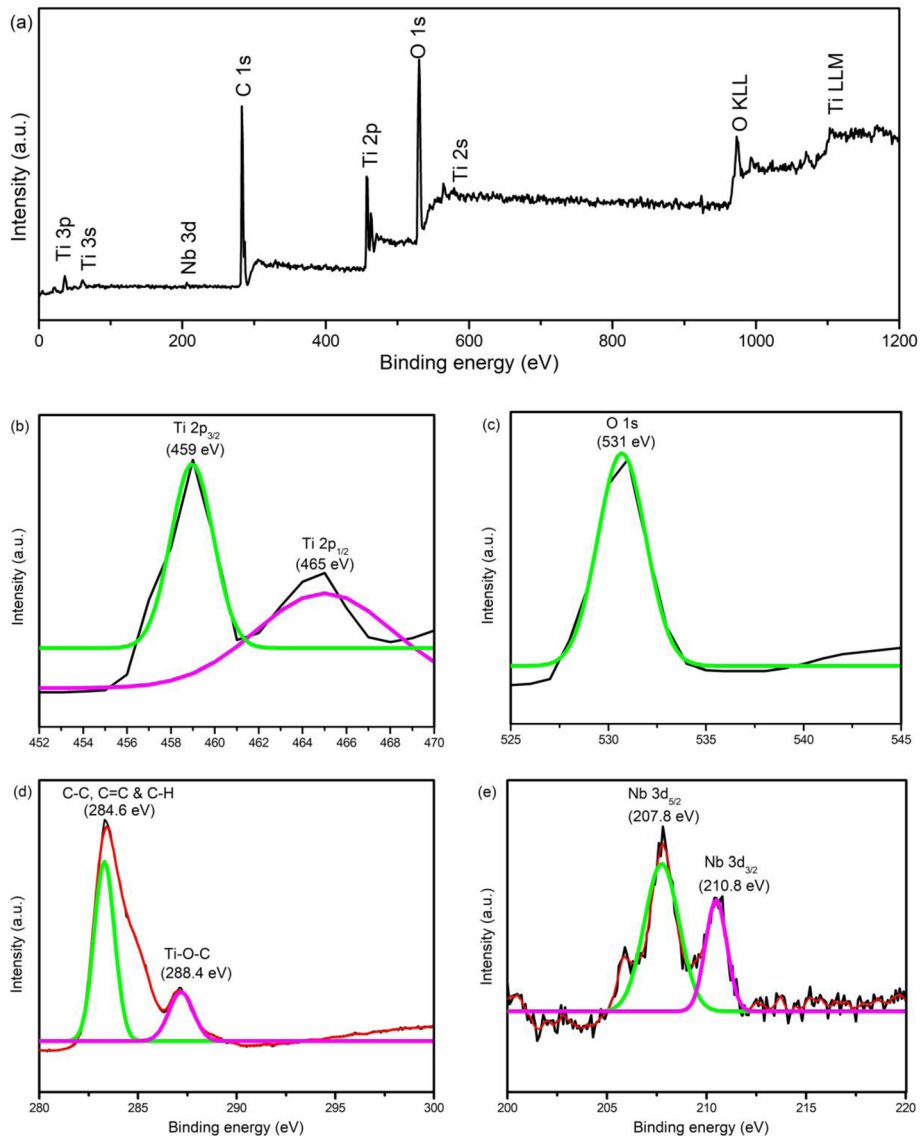

Fig. 6 XPS spectra of NTG5 **(a)** Full range spectra, **(b)** Ti 2p spectra, **(c)** O 1 s spectra, **(d)** C 1s spectra and **(e)** Nb 3d spectra

of NTG5 (Fig. 6a). As seen in Fig. 6b, the Ti 2p core level spectrum demonstrates a single pair of binding energy peaks corresponds to Ti $2p_{3/2}$ and Ti $2p_{1/2}$ which are centred at 459 and 465 eV, respectively, which clearly represents the Ti^{+4} state. The core level XPS spectra of C 1 s and O 1 s provides explicit information regarding the oxygen functional groups present in the graphene skeleton of NTG5 catalyst. A typical binding energy peak ascribed at 531 eV in O1s core level XPS spectrum (Fig. 6c) indicates the presence of metallic oxides (Ti-OH) as well as the residual –COOH [24]. In addition, according to the attained C 1 s core level spectra in Fig. 6d, the characteristic peak observed at 284.6 eV is attributed to sp^2 carbon in rGO which represents C-C, C=C, and C-H bonds. A peak at the binding energy of 288.4 eV is devoted to carboxyl carbon (O=C-O) and/or Ti-O-C group [23]. Further, it will be confirmed by the FT-IR results. As shown in Fig. 6e, Nb 3d peaks observed at 207.8 and 210.8 eV are corresponding to the Nb $3d_{5/2}$ and Nb $3d_{3/2}$ respectively. The presence of doublet represents the oxidation state of Nb as Nb^{+5}.

Raman analysis

The chemical composition of NTG5 nanocomposite was determined by correlating its Raman spectra with those of bare TiO_2 and GO. As delineated in Fig. 7a, the Raman spectral responses obtained at 402.5, 517.8 and 641.6 cm^{-1} were assigned to the B_{1g} (1), $A_{1g}B_{1g}$ (2) and E_g (2) modes of NTG5 nanocomposite, respectively, matching with the anatase structure of TiO_2 which are

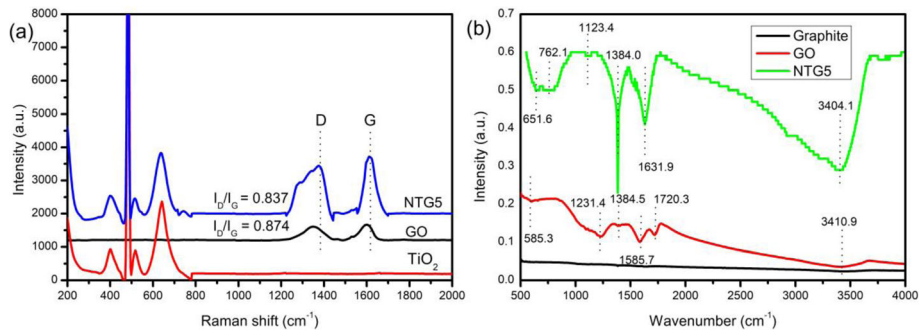

Fig. 7 **(a)** Raman spectra of TiO_2, GO and NTG5 **(b)** FT-IR spectra for Graphite, GO and NTG5

coincident with the earlier reports [25]. There are two noticeable peaks at 1350.3 and 1600.3 cm^{-1} in the GO spectrum relevant to D and G bands, respectively. On the other hand, the NTG5 nanocomposite shows these characteristic bands at 1375.6 and 1611.9 cm^{-1}. The shifting in both specified bands in the NTG5 nanocomposite compared to GO exhibits the presence of interactions between NT np's and rGO. It is worth noting that, a decrease in D/G intensity ratio was recognized for NTG5 photocatalyst (I_D/I_G = 0.837) comparing with GO (I_D/I_G = 0.874), implying that the reduction of functional groups with oxygen (hydroxyl and epoxy) and the restoration of sp^2-bonded carbons. Further, it confirms the occurrence of rGO in the NTG5 nanocomposite.

FT-IR analysis

Further, synthesized GO and NTG nanocomposites were investigated by using FT-IR spectroscopy in order to ascertain the extent of ionic interactions between GO and NT np's. And the results obtained for Graphite, GO and NTG5 nanocomposite are presented in Fig. 7b. The presence of prominent peaks of oxygen-containing functional groups like C-O-C ($U_{C\text{-}O\text{-}C}$ at 1231 cm^{-1}), C-OH ($U_{C\text{-}OH}$ at 1384 cm^{-1}), and C=O carbonyl groups ($U_{C=O}$ at 1720 cm^{-1}) in GO spectra verified that successful synthesis of hydrophilic GO by the oxidation of graphite. The broad peak at ~ 3404 cm^{-1} appeared for both GO and NTG5 nanocomposite assigned to the C-OH groups stretching vibrations and intercalated water within graphene sheets. NT np's are covalently anchored on the surface of GO through these surface functional groups through oxygen. Vibration band appearing around 1631.9 cm^{-1} in NTG5 nanocomposite assigned to the C-C vibration of graphene sheets. Significant low frequency bands corresponding to Ti-O-Ti and Ti-O-C were found around 651.6 and 762.1 cm^{-1} respectively. Thus, the obtained broad peak for the nanocomposite at the low frequency region reflects the chemical interactions between NT np's and rGO which results from the combination of Ti-O-Ti and Ti-O-C vibrations. It can be clearly understood from the spectra of GO and NTG5 composite that carbonyl (C=O) and epoxy (C-O-C) stretching peaks are faded away and identification of sharp peak for C-O band in NTG5 confirms the existence of rGO formed by the slight reduction of GO during synthesis.

PL study

The PL study of NTG nanocomposites is useful to ascertain the formation of •OH on its surface during the illumination process. The generation of •OH were examined by recording the highly fluorescent characteristic peak acquired from 2-hydroxyterephthalic acid (TAOH) which was triggered during the reactions between terephthalic acid and •OH and the experimental process is presented in SI. Fig. S2a shows the variation in the PL emission spectra of TAOH with irradiation time. A linear increase in the fluorescence intensities over the irradiation time at 420 nm was observed. Further, it is illustrated that the spectral intensity of the TAOH is increasing with an increase in •OH production which matches the former reports [26].

Usually, the generation of •OH shows a considerable positive response on the efficiency of the photocatalyst. Higher photocatalytic activity of nanocomposites can be attained with the faster generation of •OH. Fig. S2b shows PL spectral changes with the NTG nanocomposites. It can be easily understood that, the generation of •OH on the NTG nanocomposites is greater than that of NT photocatalyst. This suggests that NTG nanocomposites have higher photocatalytic activity than the NT photocatalyst. Further, it can be seen that, NTG5 nanocomposite has the strongest PL intensity, indicating a highest photocatalytic activity.

Photocatalytic degradation study

The photocatalytic activity of NTG nanocomposites was assessed by the widely accepted photocatalytic degradation reaction of RhB dye under visible light exposure. These results were compared with NT photocatalyst as a reference.

Adsorption study

Before commencing the photocatalytic degradation of RhB under visible light irradiation, the adsorption behaviour of nanocomposites determined by keeping the mixture of RhB aqueous solution and photocatalysts under dark stirring for 30 min. The extent of adsorption capacity of the photocatalyst was measured by recording absorbance of RhB dye at its characteristic wavelength 554 nm which is proportional to its concentration. Results obtained (displayed in Fig. S3) indicates that both the NTG nanocomposites and NT photocatalyst show considerable adsorption towards RhB. Increased adsorption of RhB under dark conditions (7, 22, 27 and 30% for NT, NTG1, NTG5, and NTG10, respectively) has been observed with increasing rGO concentration from 1 to 10 wt% in nanocomposites. Notably, 27% of RhB adsorbed on the NTG5 catalyst surface; in contrast, only 7% of RhB solution was adsorbed on NT catalyst. This improvement in adsorption for NTG5 nanocomposite is caused by the introduction of graphene because its crumpled surface could provide a larger surface area and mesoporosity to the catalyst. It illustrates that enhancement in adsorption of RhB dye molecules on nanocomposites results from the dispersion of NT np's on the surface of graphene, this could be resulted from π-π conjugation between RhB and aromatic regions of rGO [27]. In addition, NT np's prevent aggregation of rGO sheets on themselves during the formation of nanocomposites and it will enhance the adsorption capability of nanocomposites further. Such an intensive adsorptive nature is favourable for degradation of RhB on photocatalysts surface.

Effect of GO concentration

The photocatalytic performances of as-prepared NT, NTG1, NTG5, and NTG10 nanocomposites were assessed by the decomposition of RhB as a model pollutant under visible light illumination. Figure 8 describes that the photocatalytic decomposition curves of RhB with NT and NTG nanocomposites under the stimulation of visible light at ambient conditions. Evidently, NTG nanocomposites are exhibited better photodegradation performance than the controlled sample NT as shown in Fig. 8a due to the availability of more contact surface between NT np's and RhB dye molecules due to the incorporation of rGO [28]. From the experimental results, it can be stated that the photocatalytic efficiency following increasing trend with the amount of incorporated graphene content in nanocomposites and after optimum concentration of graphene load efficiency was decreased. It has been established clearly in the case of NTG10, after optimum concentration of rGO, the activity was decreased with further increment in GO amount. This might be due to the excessive rGO content in composite offers more opportunities for the collision of the photogenerated electron-hole pair which consequently

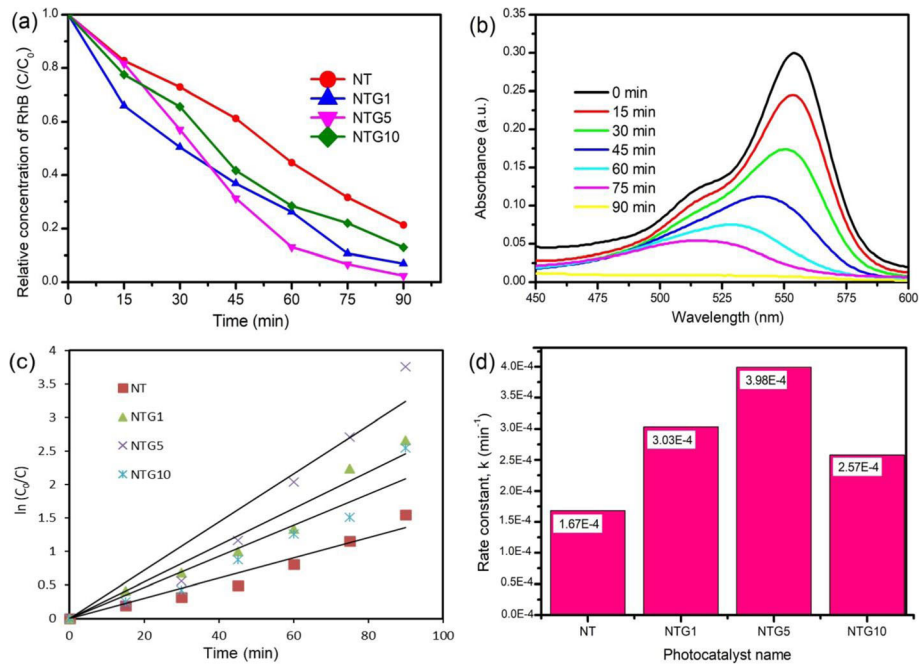

Fig. 8 **(a)** Effect of rGO loads on the degradation of RhB dye by different photocatalysts, **(b)** UV-vis absorption spectra of RhB for NTG5 nanocomposite as a function of irradiation time, **(c)** Relation between irradiation time and $\ln(c/c_0)$ and **(d)** Pseudo first-order rate constants for photocatalytic degradation experiments of RhB with different photocatalysts. Here, the solution pH = 7

encourages their recombination. Nevertheless, it also suppresses the contact surface between NT np's and RhB dye molecules resulting in lower photocatalytic performance. In particular, it has been found that NTG5 photocatalyst with 5 wt% rGO displays higher photocatalytic activity. Approximately 98% of RhB (Fig. 8b) was degraded photocatalytically with the NTG5 catalyst in 90 min under visible light stimulation followed by 93% for NTG1, 92% for NTG10 and 79% for NT.

From the plots of the degradation rate versus the illumination time (Fig. 8c), straight lines can be fitted in the first part of the plots, allowing to estimate apparent pseudo first-order kinetic constants follow the order NTG5 > NTG1 > NTG10 > NT plotted in Fig. 8d and tabulated in Table 2 [29]. The obtained photocatalytic degradation results were compared with the previously reported results and tabulated in the Table 3.

Further, on the basis of earlier studies, possible intermediates/degradation products of RhB produced during the degradation process have been proposed in the supporting information [35, 36, 37].

Effect of catalyst dosage of NTG5

To investigate the suitable catalyst concentration of NTG5 for RhB photocatalytic degradation, sequential experiments were conducted at identical conditions (RhB dye, 2 mg L^{-1}) by varying amounts of NTG5 photocatalyst from 25 to 75 mg in 100 mL of RhB dye solution. From Fig. 9a, it is evident that the degradation rates have been increased slightly with the amount of catalyst up to 50 mg and then suppresses with further increase. The predominant reason behind it is more number of catalyst active sites becoming available with an increasing amount of the catalyst which helps to adsorb more RhB dye molecules as well as to absorb more photons leading to the increase in photocatalytic behaviour of catalyst. In addition, the solution turbidity increases with further increase in higher proportions of catalyst even though more areas are available for RhB molecules for adsorption. This hinders the penetration of light through and also scatters the exposed radiation [38]. Thus, the addition of catalyst above a certain level may not contribute to excess catalytic efficiency, hence degradation rate decreases.

Table 2 Pseudo first-order kinetic rate constant (k), regression coefficient (R^2) and % of degradation of different photocatalysts for RhB dye under visible light irradiation

Photocatalyst	Rhodamine B		% of degradation
	$k \times 10^{-4}$ in min^{-1}	R^2	
NT	1.7	0.95	79
NTG1	3.0	0.96	93
NTG5	4.0	0.93	98
NTG10	2.6	0.91	92

Table 3 Comparative table for photocatalytic efficiency of NTG5 nanocomposite with the previously reported results

Nanocatalyst	Dye pollutant	% of degradation	Degradation time (min)	Reference
Nb doped TiO_2 (under UV light irrdiation)	Rhodamine B	90	60	[30]
TiO_2-GO	Methyl Orange	35	180	[31]
CdS-graphene/ TiO_2 composite	Methylene Blue	33	150	[32]
TiO_2/N-graphene nanocomposite	Eosin Y	63	180	[33]
rGO/Ag/Fe-doped TiO_2	Methylene Blue	95	150	[34]
Nb doped TiO_2/rGO nanocomposite (5 wt% GO)	Rhodamine B	98	90	Present study

Effect of dye concentration for NTG5 catalyst

The effect of RhB dye concentration on its photodegradation was deliberated by taking a fixed amount of NTG5 catalyst. From Fig. 9b, it has been described that the degradation rate increases with the increase in dye concentration from 2 to 6 mg L^{-1} and a further increment leads to a decrease in degradation rate. This might be due to the quenching of active sites on the catalyst by absorption of more dye molecules causing a decrease of the •OH generation on catalyst surface [33].

Recyclability and stability of NTG5 nanocomposite

The long-term viability of the photocatalyst for commercial applications mainly depends on the recyclability of the photocatalytic activity. In this experiment, the suspended solid (photocatalyst) in RhB dye suspension was collected from the reaction vessel and washed with Milli Q water followed by ethanol to examine the recyclability of as-synthesized NTG5 nanocomposite. The same photocatalyst was utilized for five successive trials or runs in photocatalytic degradation of RhB dye solution under similar conditions repeatedly. After every 90 min of photocatalytic reaction, the concentration of the RhB was measured. The results clearly demonstrate that the NTG5 nanocomposite has great potential for the degradation up to five successive runs without significant loss in photocatalytic activity of the photocatalyst (Fig. 10). This slight depletion in photocatalytic activity may be due to the loss of the quantity of catalyst during washing and adhesion of dye molecules on the surface of the photocatalyst. After examination of the recyclability of tested nanocomposite, collected and checked its stability by characterizing with XRD and FT-IR. The XRD and FT-IR patterns are similar even after five successive

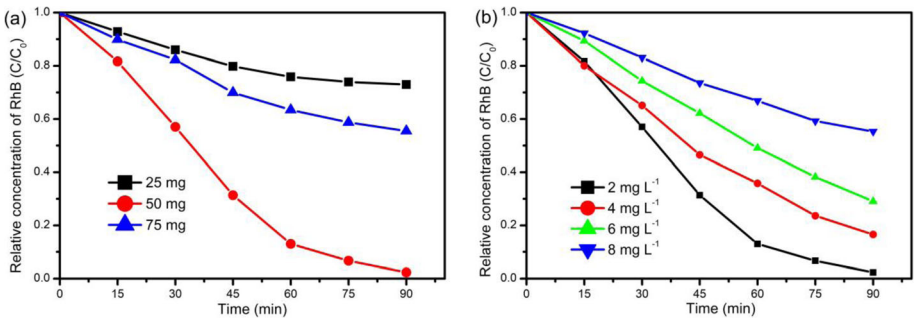

Fig. 9 (a) Effect of catalyst dosage on photodegradation of RhB and **(b)** Effect of initial concentration of RhB on photodegradation. Here, the solution pH = 7

runs completed when compared with the prepared NTG5 nanocomposite (Fig. S4a and b). This indicates that the synthesized NTG5 nanocomposite is stable photocatalyst and reusable for successive five runs.

By considering all the above facts, it has been found that numerous factors play a significant role to achieve better photocatalytic efficiency of NTG5 nanocomposite under visible light irradiation. This includes adsorption capacity, light absorption behaviour, and effective charge separation ability through an interface of photocatalysts, which are explained below:

1) The larger surface area of catalyst helps to interact more dye molecules through aromatic regions of rGO on NTG nanocomposites [28].
2) The existing Ti–O–C chemical bond at the interface between NT np's and rGO can narrow the band gap of TiO_2 and extend the photo-responding range.
3) Lengthening of e^--h^+ pair separation by electron insertion through interfacial chemical linkage (Ti-O-C), which greatly suppresses their combination e^--h^+ pair in the excited TiO_2 [19, 27].

During the photoreaction, the promotion of electron takes place from valence band to conduction band on the TiO_2 surface under visible light exposure. In the present catalyst system, dopant Niobium (Nb) can create a transitional energy state between the aforementioned two bands of TiO_2 which can effectively reduce the band gap energy of TiO_2. It is renowned that graphene can also generate e^--h^+ pairs under visible light exposure, these electrons from graphene surface can enter into the TiO_2 conduction band through π-π conjugation and vice versa. Further, the electron cloud on TiO_2 conduction band and rGO surface could produce •OH through superoxide formation by reaction with adsorbed oxygen on nanocomposites surface while the hole in the valence band also can generate •OH by reaction with water or OH^- that are absorbed on the surface of the catalyst. These generated •OH are the most powerful tools to decompose the organic pollutants into CO_2, and H_2O. Based on the experimental results, a possible

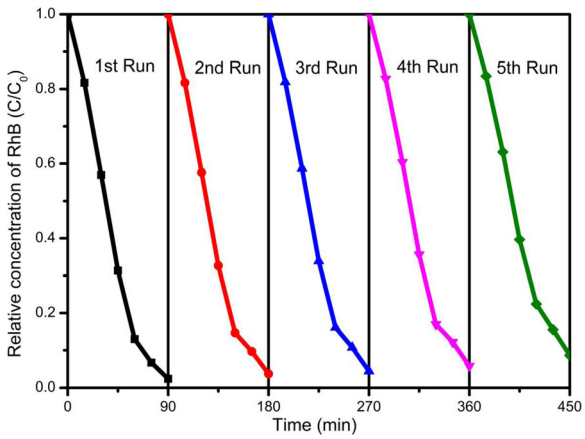

Fig. 10 Recyclability test of NTG5 nanocomposite for consecutive reaction cycles

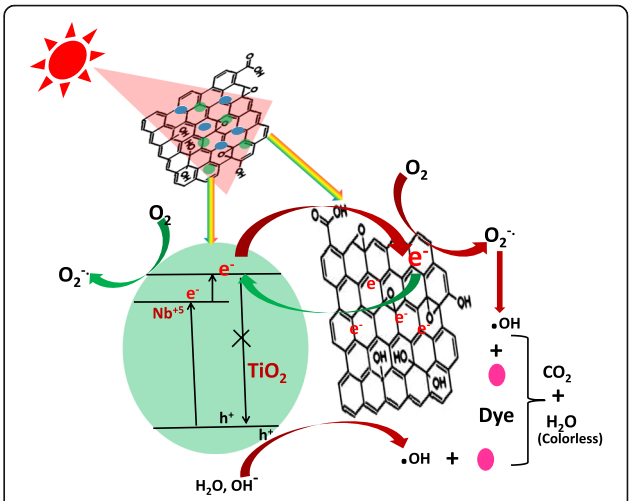

Fig. 11 Schematic representation for degradation of RhB dye on Nb doped TiO_2/rGO nanocomposites

mechanism was proposed in an earlier reported publication from our group [18] as shown in Fig. 11.

Conclusions

The Nb doped TiO_2/rGO nanocomposites were successfully synthesized via in situ process by modified sol-gel method at room temperatures. The formation of the Nb doped TiO_2 nanoparticles and their incorporation on the rGO nanosheets surface was established by XRD, TEM, SEM-EDX, and UV-DRS techniques. Furthermore, experimental results clearly recommended that there is a significant interaction between rGO and Nb doped TiO_2 nanoparticles. Thereafter, the influence of different operating factors such as GO concentration, catalyst loadings and dye concentration on photocatalytic degradation of RhB was demonstrated under visible light irradiation. These exercises confessed that GO concentration in Nb doped TiO_2 nanoparticles helps in the enhancement of RhB dye molecules adsorption in dark condition as well as observed an appreciable change in photodegradation efficiency was achieved compared with NT nanoparticles. The NTG5 exhibits greater photocatalytic efficiency towards RhB about 98% within 90 min among all the catalysts under visible light irradiation. Based on its excellent photocatalytic activity, stability and recyclability shows that NTG nanocomposites are promising materials for various practical applications in the field of photocatalysis and wastewater remediation.

Supplementary Information

The online version contains supplementary material available at https://doi.org/10.1186/s42834-021-00110-x.

Additional file 1.

Acknowledgments

This work has been supported by the University Grants Commission, New Delhi, India for financial support in the form of JRF.

Authors' contributions

NP: conceptualization, experimentation, data interpretation and writing-original draft; TSR: supervision and writing-original draft; IMR: data interpretation and assisted in draft writing & editing; KVDL, GD, GJ and SAA: writing-review & editing. All authors read and approved the final manuscript.

Funding

Not Applicable.

Availability of data and materials

All data generated or analyzed during this study are included in this published article [and supplementary information file].

Declarations

Competing interests

The authors declare that no competing interests.

Received: 24 February 2021 Accepted: 15 October 2021
Published online: 20 November 2021

References

1. Bes-Pia A, Mendoza-Roca JA, Alcaina-Miranda MI, Iborra-Clar A, Iborra-Clar MI. Reuse of wastewater of the textile industry after its treatment with a combination of physico-chemical treatment and membrane technologies. Desalination. 2002;149:169–74.
2. Botsa SM, Basavaiah K. Fabrication of multifunctional TANI/Cu_2O/Ag nanocomposite for environmental abatement. Sci Rep-UK 2020;10:14080.
3. Vamathevan V, Amal R, Beydoun D, Low G, McEvoy S. Photocatalytic oxidation of organics in water using pure and silver-modified titanium dioxide particles. J Photoch Photobio A 2002;148:233–45.
4. Leary R, Westwood A. Carbonaceous nanomaterials for the enhancement of TiO_2 photocatalysis. Carbon. 2011;49:741–72.
5. Mulpuri RK, Tirukkovalluri SR, Imandi MR, Alim SA, Kapuganti VDL. Zinc and boron co-doped nanotitania with enhanced photocatalytic degradation of Acid Red 6A under visible light irradiation. Sustain Environ Res 2019;29:29.
6. Miditana SR, Tirukkovalluri SR, Raju IM, Alim SA, Jaishree G, Chippada MLVP. Gemini surfactant assisted synthesis of mesoporous Mn/Mg bimetal doped TiO_2 nanomaterial: characterization and photocatalytic activity studies under visible light irradiation. Sustain Environ Res 2021;31:6.
7. Padmaja JS, Rao TS, Lakshmi KVD, Raju IM. Fabrication of hetero-structured mesoporours TiO_2-$SrTiO_3$ nanocomposite in presence of Gemini surfactant: characterization and application in catalytic degradation of Acid Orange. J Environ Chem Eng 2018;6:6457–67.
8. Chandra MR, Rao TS, Kim HS, Pammi SVN, Prabhakarrao N, Raju IM. Hybrid copper doped titania/polythiophene nanorods as efficient visible light-driven photocatalyst for degradation of organic pollutants. J Asian Ceram Soc 2017;5:436–43.
9. Raju IM, Rao TS, Lakshmi KVD, Chandra MR, Padmaja JS, Divya G. Poly 3-Thenoic acid sensitized, Copper doped anatase/brookite TiO_2 nanohybrids for enhanced photocatalytic degradation of an organophosphorus pesticide. J Environ Chem Eng 2019;7:103211.
10. Wang P, Han L, Zhu CZ, Zhai YM, Dong SJ. Aqueous-phase synthesis of Ag-TiO_2-reduced graphene oxide and Pt-TiO_2-reduced graphene oxide hybrid nanostructures and their catalytic properties. Nano Res 2011;4:1153–62.
11. Botsa SM, Naidu GP, Ravichandra M, Rani SJ, Anjaneyulu RB, Ramana CV. Flower like SnO_2-Fe_2O_3-rGO ternary composite as highly efficient visible light induced photocatalyst for the degradation of organic pollutants from contaminated water. J Mater Res Technol 2020;9:12461–72.
12. Yang JK, Zhang XT, Wang CH, Sun PP, Wang LL, Xia B, et al. Solar photocatalytic activities of porous Nb-doped TiO_2 microspheres prepared by ultrasonic spray pyrolysis. Solid State Sci 2012;14:139–44.
13. Choi WY, Termin A, Hoffmann MR. The role of metal ion dopants in quantum-sized TiO_2: correlation between photoreactivity and charge carrier recombination dynamics. J Phys Chem-US 1994;98:13669–79.
14. Woan K, Pyrgiotakis G, Sigmund W. Photocatalytic carbon-nanotube-TiO_2 composites. Adv Mater 2009;21:2233–9.
15. Allen MJ, Tung VC, Kaner RB. Honeycomb carbon: a review of graphene. Chem Rev 2010;110:132–45.
16. Liu ZH, Wang ZM, Yang XJ, Ooi KT. Intercalation of organic ammonium ions into layered graphite oxide. Langmuir. 2002;18:4926–32.
17. Hummers WS, Offeman RE. Preparation of graphitic oxide. J Am Chem Soc 1958;80:1339.
18. Prabhakarrao N, Chandra MR, Rao TS. Synthesis of Zr doped TiO_2/reduced graphene oxide (rGO) nanocomposite material for efficient photocatalytic degradation of Eosin Blue dye under visible light irradiation. J Alloys Compd 2017;694:596–606.
19. Zhang YH, Tang ZR, Fu X, Xu YJ. Engineering the unique 2D mat of graphene to achieve graphene-TiO_2 nanocomposite for photocatalytic selective transformation: what advantage does graphene have over its forebear carbon nanotube? ACS Nano 2011;5:7426–35.
20. Dai K, Lu LH, Liu Q, Zhu GP, Liu QZ, Liu ZL. Graphene oxide capturing surface-fluorinated TiO_2 nanosheets for advanced photocatalysis and the reveal of synergism reinforce mechanism. Dalton T. 2014;43:2202–10.
21. Meyer JC, Geim AK, Katsnelson MI, Novoselov KS, Booth TJ, Roth S. The structure of suspended graphene sheets. Nature. 2007;446:60–3.
22. Wang HL, Robinson JT, Diankov G, Dai HJ. Nanocrystal growth on graphene with various degrees of oxidation. J Am Chem Soc 2010;132:3270–1.

23. Sing KSW, Everett DH, Haul RAW, Moscou L, Pierotti RA, Rouquerol J, et al. Reporting physisorption data for gas/solid systems with special reference to the determination of surface area and porosity (recommendations 1984). Pure Appl Chem 1985;57:603–19.
24. Park G, Bartolome L, Lee KG, Lee SJ, Kim DH, Park TJ. One-step sonochemical synthesis of a graphene oxide-manganese oxide nanocomposite for catalytic glycolysis of poly (ethylene terephthalate). Nanoscale. 2012;4:3879–85.
25. Li N, Liu G, Zhen C, Li F, Zhang LL, Cheng HM. Battery performance and photocatalytic activity of mesoporous anatase TiO_2 nanospheres/graphene composites by template-free self-assembly. Adv Funct Mater 2011;21:1717–22.
26. Yu JG, Xiang QJ, Zhou MH. Preparation, characterization and visible-light-driven photocatalytic activity of Fe-doped titania nanorods and first-principles study for electronic structures. Appl Catal B-Environ 2009;90:595–602.
27. Pan X, Zhao Y, Liu S, Korzeniewski CL, Wang S, Fan ZY. Comparing graphene-Tio_2 nanowire and graphene-TiO_2 nanoparticle composite photocatalysts. ACS Appl Mater Interfaces 2012;4:3944–50.
28. Perera SD, Mariano RG, Vu K, Nour N, Seitz O, Chabal Y, et al. Hydrothermal synthesis of graphene-TiO_2 nanotube composites with enhanced photocatalytic activity. ACS Catal 2012;2:949–56.
29. Kim SY, Lim TH, Chang TS, Shin CH. Photocatalysis of methylene blue on titanium dioxide nanoparticles synthesized by modified sol-hydrothermal process of $TiCl_4$. Catal Lett 2007;117:112-8.
30. Baral A, Das DP, Minakshi M, Ghosh MK, Padhi DK. Probing environmental remediation of RhB organic dye using α-MnO_2 under visible-light irradiation: structural, photocatalytic and mineralization studies. ChemistrySelect. 2016;1:4277–85.
31. Xiao X, Ma XL, Liu ZY, Li WW, Yuan H, Ma XB, et al. Degradation of rhodamine B in a novel bio-photoelectric reductive system composed of *Shewanella oneidensis* MR-1 and Ag_3PO_4. Environ Int 2019;126:560–7.
32. Liang LP, Cheng LB, Zhang YT, Wang Q, Wu Q, Xue YY, et al. Efficiency and mechanisms of rhodamine B degradation in Fenton-like systems based on zero-valent iron. RSC Adv 2020;10:28509–15.
33. Daneshvar N, Salari D, Khataee AR. Photocatalytic degradation of azo dye acid red 14 in water: investigation of the effect of operational parameters. J Photoch Photobio A 2003;157:111–6.
34. Wang HY, Chen JZ, Xiao FX, Zheng JW, Liu B. Doping-induced structural evolution from rutile to anatase: formation of Nb-doped anatase TiO_2 nanosheets with high photocatalytic activity. J Mater Chem A 2016;4:6926–32.
35. Chen C, Cai WM, Long MC, Zhou BX, Wu YH, Wu DY, et al. Synthesis of visible-light responsive graphene oxide/TiO_2 composites with p/n heterojunction. ACS Nano 2010;4:6425–32.
36. Park CY, Kefayat U, Vikram N, Ghosh T, Oh WC, Cho KY. Preparation of novel CdS-graphene/TiO_2 composites with high photocatalytic activity for methylene blue dye under visible light. B Mater Sci 2013;36:869–76.
37. Liu YL, Pei FY, Lu RJ, Xu SG, Cao SK. TiO_2/N-graphene nanocomposite via a facile in-situ hydrothermal sol-gel strategy for visible light photodegradation of eosin Y. Mater Res Bull 2014;60:188–94.
38. Jaihindh DP, Chen CC, Fu YP. Reduced graphene oxide-supported Ag-loaded Fe-doped TiO_2 for the degradation mechanism of methylene blue and its electrochemical properties. RSC Adv 2018;8:6488–501.

Publisher's Note